Report LR-540

On the Buckling of Axially Compressed Imperfect Orthotropic Shells with Elastic Edge Supports

March 1988

J. Arbocz / P.G. Vermeulen / J. van Geer

TU Delft
Delft University of Technology

Faculty of Aerospace Engineering

On the Buckling of Axially Compressed Imperfect Orthotropic Shells with Elastic Edge Supports

J. Arbocz/P.G. Vermeulen/J. van Geer

TABLE OF CONTENTS

LIST OF SYMBOLS

a	radius of ring centerline
A	cross-sectional area of stringer
a_{ij}	stiffness coefficients in Eqs. 16, 17 and 18
b_{ij}	flexibility coefficients in Eqs. 19, 20 and 21
B_i, B_i	Coefficients in Eqs 24 and 25, respectively
c	$= \sqrt{3(1-\nu^2)}$
C	ring size parameter, see figure 10
D	$= Et^3/(4c^2)$, bending stiffness of shell wall
$\bar{D}_{ij}$	nondimensional effective bending stiffness
E	Young's modulus
e_x, e_z	eccentricity of ring centroid, see figure 7
F, f_i	Airy stress functions (i=0,1,2)
F_x, F_y, F_z	force resultants on the ring
G	shear modulus
H, H_o, H_1	generalized tranverse shear resultants, see Eqs. (6, 9) and figure 7
H_{xx}	effective stretching stiffness
$\bar{H}_{xx}$	nondimensional effective stretching stiffness
I_x, I_z	moment of inertia of the endring
I_{xz}	product of inertia of the endring
J	torsional constant
n	number of full waves in the circumferential direction
N_o	applied compressive line load (N/mm)
N_x, N_y, N_{xy}	stress resultants (N/mm)
N_{x_M}	perfect shell buckling load using membrane prebuckling analysis
M_x, M_y, M_{xy}	moment resultants (mm * N/mm)
M_t	torsional moment resultant on the ring
$\bar{Q}_{xx}$	nondimensional effective torsional stiffness
q	load eccentricity from shell wall midsurface positive inward
$\bar{q}$	$= \frac{4cR}{t^2} q$, dimensional load eccentricity
R	radius of schell
t	wall thickness of shell
u, v	in-plane displacements

W, w_o, w_1	radial displacement, positive inward
$\bar{W}$, A_o, A_1	radial imperfection from perfect cylinder
W_ν	Poisson's expansion ($= -\frac{\nu}{c}\frac{\bar{H}_{xx}}{(1+\mu_1)}\lambda$)
$\hat{W}$	normalized buckling modes, figures 12, 13 and 14
x, y	axial and circumferential coordinates on the middle surface of the shell, respectively
$\bar{x}$, $\bar{y}$	nondimensional coordinates $\frac{x}{R}$ and $\frac{y}{R}$, respectively
Y	unified vector variable, eq. (26)
z	radial coordinate, positive inward
β_x, β_y, β_z	rotation of ring coordinates
θ	$= Y/R$
λ	nondimensional loading parameter ($= \frac{cR}{Et^2} N_o$)
λ_s	value of λ at the limit point
ν	Poisson's ratio
ρ	normalized nondimensional loading parameter (N_x/N_{x_M}) where N_{x_M} depends on the boundary condition used
ρ_s	normalized nondimensional collapse load parameter of the imperfect shell (value of ρ at the limit point)
ρ_{exp}	normalized nondimensional experimental collapse load parameter

Superscripts

r	ring
s	shell

ON THE BUCKLING OF AXIALLY COMPRESSED IMPERFECT ORTHOTROPIC SHELLS WITH ELASTIC EDGE SUPPORTS

J. ARBOCZ[1], P.G. VERMEULEN[2] and J. VAN GEER[1]

[1] Aeronautics Faculty, TU-Delft (The Netherlands)

[2] N.I.V.R., TU-Delft (The Netherlands)

SUMMARY

A rigorous solution is presented for the case of axially compressed stiffened cylindrical shells with general imperfections, where the edge supports are provided by symmetrical or unsymmetrical elastic rings. The circumferential dependence is eliminated by a truncated Fourier series. The resulting nonlinear 2-point boundary value problem is solved numerically via the 'Shooting Method'. The changing deformation patterns resulting from the different degrees of interaction between the given initial imperfections and the specified end rings are displayed. Recommendations are made as to the minimum stiffnesses required for optimal load carrying configurations.

INTRODUCTION

Since thinwalled structures exhibit very favorable strength over weight ratios the design of stiffened or unstiffened shells continue to play an important role in modern engineering. Unfortunately, thinwalled shells are prone to buckling instabilities.

In the last decades initial geometric imperfections [1]-[2] and general elastic supports [3] have been widely accepted as the explanation for the wide experimental scatter and the poor correlation between the predictions based on a linearized small deflection theory with SS-3 ($N_x = v = w = M_x = 0$) boundary conditions and the experimental values.

The effect of different combinations of in-plane boundary conditions on the stability of axially compressed perfect shells or shells with axisymmetric imperfections have been studied analytically and numerically by Hoff [4] and Almroth [5]. Recently Singer and his coworkers [3] have developed an experimental technique which makes it possible to estimate the degree of elastic support present in a particular test set-up.

Despite all these theoretical and experimental results the shell design manuals in use at the present time adhere to the so-called 'Lower Bound Design Philosophy', which involves the use of a so-called 'knockdown factor'. The empirical 'knockdown factor γ' is so chosen that when it is multiplied with the

buckling load of the perfect structure P_c a lower bound to all available experimental data is obtained.

It has been hoped that with the large scale introduction of computer codes with advanced nonlinear capabilities an alternate design procedure could be developed which would no longer penalize innovative shell design because of the poor experimental results obtained elsewhere.

As a step towards this goal Arbocz [6] in 1984 published the results of an extensive numerical study of the well characterized stringer stiffened shell AS-2, which has been tested at Caltech in 1970 [7].

Using an early finite difference version of the well known nonlinear shell code STAGS [8] the complete shell was modeled. The measured initial imperfections were fitted by a bivariate cubic spline fit. This model was then used to compute the first derivatives of the measured initial imperfections with respect to x and θ at all nodal points. Employing C-4 ($u = v = w = w_{,x} = 0$) boundary conditions an iterative step-by-step procedure then located the limit point of the prebuckling states. The calculated collapse load of ρ_s=0.8563 has been normalized by -320.8 N/cm, the buckling load of the perfect shell using membrane prebuckling and the same C-4 boundary conditions. The calculated collapse load is unexpectedly high since the shell AS-2 buckled at ρ_{exp}=0.715.

In looking for an explanation, a comparison of the calculated prebuckling deformation for C-4 boundary conditions (see Fig. 1) with the experimentally measured prebuckling deformation (see Fig. 2) is helpful.

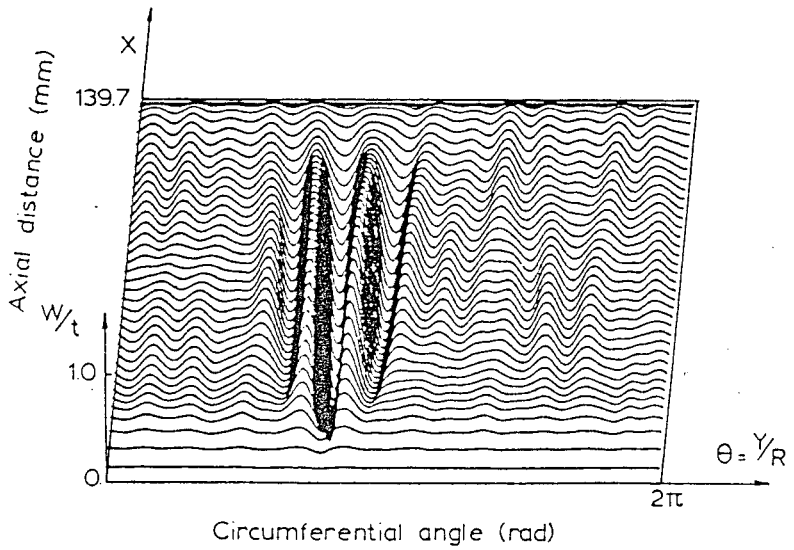

Fig. 1. Calculated prebuckling growth of the stringer stiffened shell AS-2 at ρ_s=0.8563 (41 x 161 = 6601 mesh points).
(Boundary conditions: $u = v = w = w_{,x} = 0$).

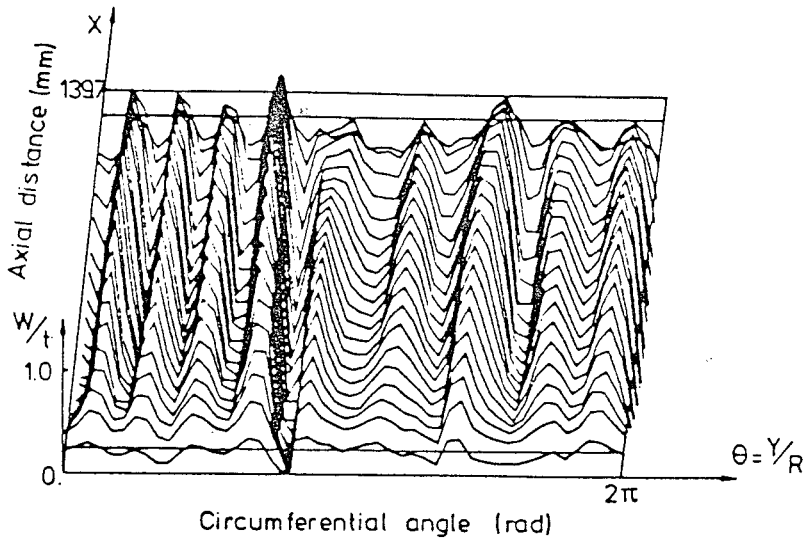

Fig. 2. Measured prebuckling growth of the stringer stiffened shell AS-2 at ρ=0.629 (21 x 49 = 1029 data points).

After looking at these figures it is obvious that the two deformation patterns are strikingly different. Since the measured initial imperfections are modeled quite accurately by the bivariate cubic spline fit used, therefore the answer must be sought in a possible difference between the C-4 boundary conditions used with the numerical calculations and the actual elastic boundary conditions present at the experimental set-up.

This statement is reinforced by the results shown in Figures 3 and 4 of rerunning the current discrete model using the same spline fitted initial imperfections as input but changing the boundary conditions successively to C-3 ($N_x = v = w = w,_x = 0$) and to SS-3 ($N_x = v = w = M_x = 0$).

It must be mentioned here that for the C-3 boundary conditions the limit load ρ_s=0.8153 is normalized by -256.9 N/cm, whereas for the SS-3 boundary conditions the limit load ρ_s=0.8095 is normalized by -229.8 N/cm. These normalizing factors are the bifurcation buckling loads of the perfect AS-2 shell using membrane prebuckling and the indicated boundary conditions.

From a comparison of the calculated prebuckling deformations using the same initial imperfections but different boundary conditions with the experimentally measured prebuckling growth it appears that the best agreement occurs for the SS-3 boundary conditions.

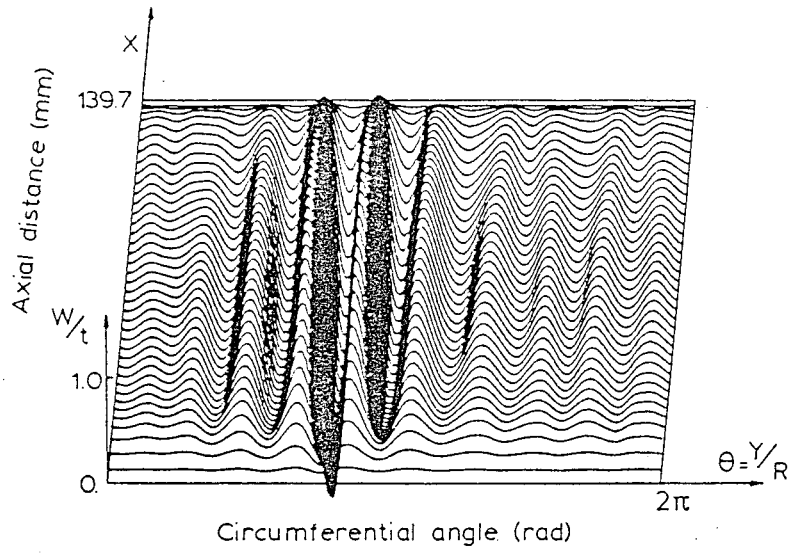

Fig. 3. Calculated prebuckling growth of the stringer stiffened shell AS-2 at ρ_s=0.8153 (41 x 161 = 6601 mesh points).
(Boundary conditions: $N_x = v = w = w_{,x} = 0$).

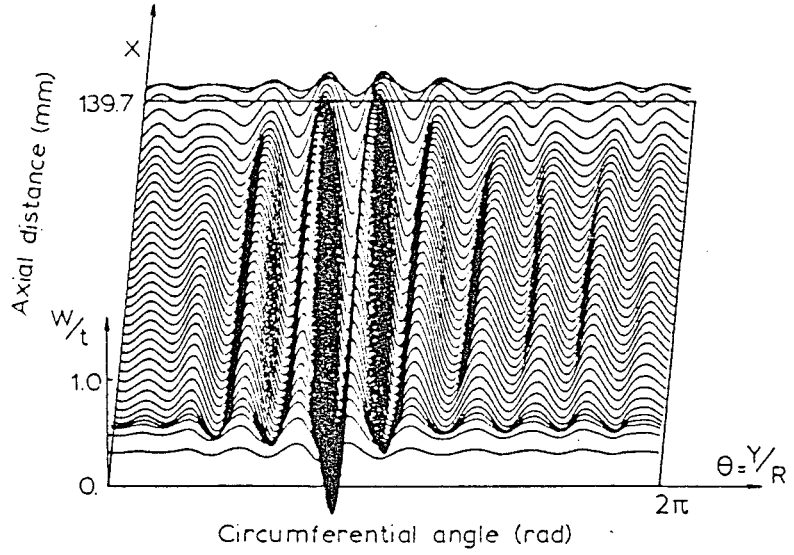

Fig. 4. Calculated prebuckling growth of the stringer stiffened shell AS-2 at ρ_s=0.8095 (41 x 161 = 6601 mesh points).
(Boundary conditions: $N_x = v = w = M_x = 0$).

Thus it is clear that in order to reproduce the buckling behaviour of the imperfect shell AS-2 accurately one must not only include the measured initial imperfections but also model the experimental boundary conditions more realistically.

THEORETICAL ANALYSIS

In an effort to gain insight into the possible nonlinear interaction between elastic boundary conditions and the initial imperfections the following analytical investigation is carried out, whereby the elastic boundary conditions are modeled by attaching rings of general cross-sectional shape eccentrically at the shell edges. The sign convention used for shell and ring analysis is shown in Fig. 5. For the shell analysis the Donnell type nonlinear shell equations from Ref. [9] are used, whereas the ring analysis is based on Cohen's ring equations [10]. Whenever necessary the corresponding variables will be distinguished by superscripts $(\ )^s$ for shell variables and by superscripts $(\ )^r$ for ring variables.

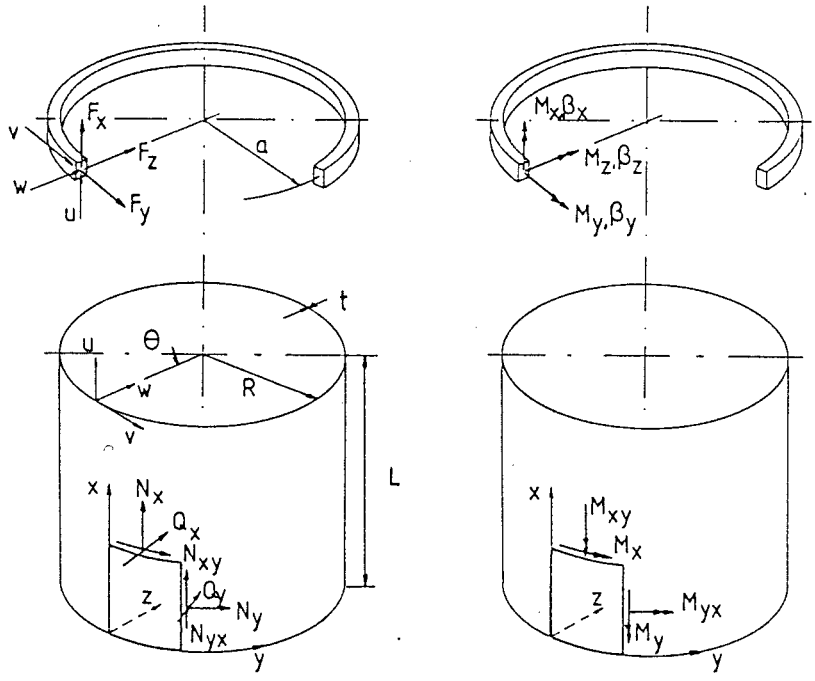

Fig. 5. Sign convention used for shell and ring analysis.

In order to be able to satisfy the displacement compatibility conditions between the end-rings and the edges of the shell, one must express the ring displacements in the same form as the one assumed for the shell displacements. Further the expansion assumed for the load terms must not only be consistent with the terms assumed for the displacements but they must also form a self-equilibrating force system. Thus the Fourier decomposition of the ring equations will be based on the following expressions

$$
\begin{aligned}
u^r &= u_0^r + u_1^r \cos n\theta + u_2^r \cos 2n\theta \\
v^r &= v_1^r \sin n\theta + v_2^r \sin 2n\theta \\
w^r &= w_o^r + w_1^r \cos n\theta \\
\beta_y^r &= \beta_{y_0}^r + \beta_{y_1}^r \cos n\theta
\end{aligned}
\qquad (1)
$$

and

$$
\begin{aligned}
F_x &= F_{x_1} \cos n\theta + F_{x_2} \cos 2n\theta \\
F_y &= F_{y_1} \sin n\theta + F_{y_2} \sin 2n\theta \\
F_z &= F_{z_0} + F_{z_1} \cos n\theta \\
M_t &= M_{t_0} + M_{t_1} \cos n\theta
\end{aligned}
\qquad (2)
$$

See Figure 6 for the sign convention used.

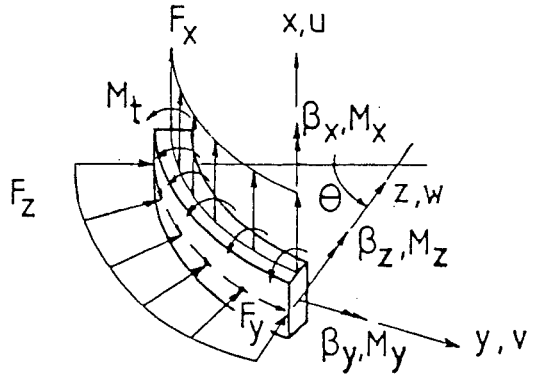

Fig. 6. Forces acting on a ring segment.

Substituting these expressions into Cohen's ring equations and equating coefficients of like terms results in the following separated set of Cohen's ring equations:

For n=0

$$\frac{1}{a^3}\begin{bmatrix} a^2EA & 0 \\ 0 & aEI_z \end{bmatrix}\begin{bmatrix} w_0 \\ \beta_{y_0} \end{bmatrix} = \begin{bmatrix} aF_{z_0} \\ M_{t_0} \end{bmatrix} \tag{3}$$

For n≧2

$$\frac{1}{a^3}\begin{bmatrix} n^2(n^2EI_z+GJ) & -n^3EI_{xz} \\ -n^3EI_{xz} & n^2(EI_x+a^2EA) \\ n^4EI_{xz} & -n(n^2EI_x+a^2EA) \\ n^2(EI_z+GJ) & -nEI_{xz} \end{bmatrix} \tag{4}$$

$$\begin{bmatrix} n^4EI_{xz} & n^2a(EI_z+GJ) \\ -n(n^2EI_x+a^2EA) & -naEI_{xz} \\ n^4EI_x+a^2EA & n^2aEI_{xz} \\ n^2EI_{xz} & a(EI_z+n^2GJ) \end{bmatrix}\begin{bmatrix} u_1 \\ v_1 \\ w_1 \\ \beta_{y_1} \end{bmatrix} = \begin{bmatrix} aF_{x_1} \\ aF_{y_1} \\ aF_{z_1} \\ M_{t_1} \end{bmatrix}$$

and

$$\frac{1}{a^3}\begin{bmatrix} 4n^2(4n^2EI_z+GJ) & -8n^3EI_{xz} \\ -8n^3EI_{xz} & 4n^2(EI_x+a^2EA) \end{bmatrix}\begin{bmatrix} u_2 \\ v_2 \end{bmatrix} = \begin{bmatrix} aF_{x_2} \\ aF_{y_2} \end{bmatrix} \tag{5}$$

Next one must express the line loads and the torsional moment acting at the ring centroid in terms of the stress- and moment resultants of the shell edge attached to it. Considering the free body diagrams at x=0 shown in Fig. 7 one obtains the following relationships

$$\begin{aligned} F_x^r a &= N_x^s R + N_o(R-q) \\ F_y^r a &= N_{xy}^s R \\ F_z^r a &= H^s R \\ M_t^r a &= M_x^s R + e_x H^s R - e_z N_x^s R + (q-e_z)\, N_o(R-q) \end{aligned} \tag{6}$$

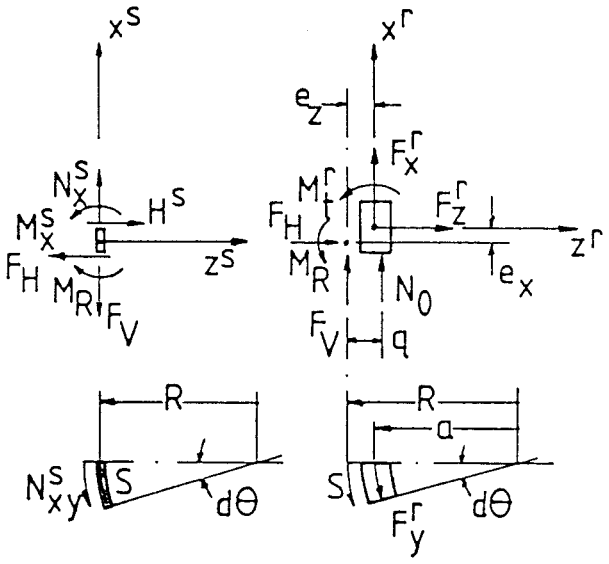

Fig. 7. Determination of forces and moments at the ring centroid.

At the upper edge (at x=L) one obtains the same expressions except for a minus sign in front of the terms on the right hand side. Notice that N_o is the external compressive line load applied at a distance q from the shell mid-surface.

Considering now the compatibility at the ring centroid of the ring and shell displacements and rotations yields the following expressions at the lower edge (at x=0)

$$\begin{aligned} u^r &= u^s - e_z\, w^s_{,x} \\ v^r &= \frac{a}{R}\, v^s - e_x\, u^s_{,y} - e_z\, w^s_{,y} \\ w^r &= w^s + e_x\, w^s_{,x} \\ \beta^r_y &= -w^s_{,x} \end{aligned} \tag{7}$$

Notice that at the upper edge (at x=L) identical expressions are obtained.

Using the previously shown Fourier decomposition of the ring variables (Eqs. 1-2) and the following Fourier decomposition of the shell variables

$$\begin{aligned} u^s &= t\,(u^s_o + u^s_1 \cos n\theta + u^s_2 \cos 2n\theta) \\ v^s &= t(v^s_1 \sin n\theta + v^s_2 \sin 2n\theta) \\ w^s &= t(W_v + w^s_0 + w^s_1 \cos n\theta) \\ w^s_{,x} &= t(w^s_{0,x} + w^s_{1,x} \cos n\theta) \end{aligned} \tag{8}$$

and

$$N_x^s = \frac{Et^2}{cR}\,(-\lambda + N_{x_1}^s \cos n\theta + N_{x_2}^s \cos 2n\theta)$$

$$N_{xy}^s = \frac{Et^2}{cR}\,(N_{xy_1}^s \sin n\theta + N_{xy_2}^s \sin 2n\theta)$$

$$H^s = \frac{t}{R^3}\,D\,(H_0^s + H_1^s \cos n\theta) \qquad (9)$$

$$M_x^s = \frac{t}{R^2}\,D\,(M_{x_0}^s + M_{x_1}^s \cos n\theta)$$

where

$$D = \frac{Et^3}{4c^2} \qquad \text{and} \qquad c = \sqrt{3(1-\nu^2)}$$

One obtains upon substitution and equating coefficients of like terms the following separated form of the forces and moments at the ring centroid at the lower edge (at x=0)

For n=0

$$aF_{z_0}^r = \frac{t}{R^2}\,D\,H_0^s$$

$$aM_{t_0}^r = e_x \frac{t}{R^2}\,D\,H_0^s + \frac{t}{R}\,D\,M_{x_0}^s + N_o R_q \qquad (10)$$

For n ≥2

$$aF_{x_1}^r = \frac{Et^2}{c}\,N_{x_1}^s$$

$$aF_{y_1}^r = \frac{Et^2}{c}\,N_{xy_1}^s$$

$$aF_{z_1}^r = \frac{t}{R^2}\,D\,H_1^s \qquad (11)$$

$$aM_{t_1}^r = -e_z \frac{Et^2}{c}\,N_{x_1}^s + e_x \frac{t}{R^2}\,D\,H_1^s + \frac{t}{R}\,D\,M_{x_1}^s$$

and

$$aF^r_{x_2} = \frac{Et^2}{c} N^s_{x_2}$$

$$aF^r_{y_2} = \frac{Et^2}{c} N^s_{xy_2} \tag{12}$$

and the following separated form of the displacement and rotation compatibility conditions

For n=0

$$u^r_0 = t(u^s_0 - e_z w^s_{0,x})$$

$$w^r_0 = t(W_v + w^s_0 + e_x w^s_{0,x}) \tag{13}$$

$$\beta^r_{y_0} = -t\, w^s_{0,x}$$

For n≥2

$$u^r_1 = t(u^s_1 - e_z w^s_{1,x})$$

$$v^r_1 = t(n \frac{e_x}{R} u^s_1 + \frac{a}{R} v^s_1 + n \frac{e_z}{R} w^s_1) \tag{14}$$

$$w^r_1 = t(w^s_1 + e_x w^s_{1,x})$$

$$\beta^r_{y_1} = - t\, w^s_{1,x}$$

and

$$u^r_2 = t u^s_2$$

$$v^r_2 = t(2n \frac{e_x}{R} u^s_2 + \frac{a}{R} v^s_2) \tag{15}$$

Substituting now in the separated form of Cohen's ring equations (Eqs. 3-5) for the ring displacements and the ring forces their equivalents in terms of the shell variables (Eqs. 10-15) yields the general elastic boundary conditions, which can be expressed in two different forms, namely

the general elastic boundary conditions valid in the limit as $E_r \to 0$ (free edges)

For n=0

$$\begin{aligned} a^o_{11}\,(w^s_0 + W_\nu) + a^o_{12}\,w^s_{0,x} &= H^s_o \\ a^o_{21}\,(w^s_0 + W_\nu) + a^o_{22}\,w^s_{0,x} &= M^s_{x_0} + \lambda\bar{q} \end{aligned} \tag{16}$$

For n≥2

$$\begin{aligned} a^1_{11}\,u^s_1 + a^1_{12}\,v^s_1 + a^1_{13}\,w^s_1 + a^1_{14}\,w^s_{1,x} &= N^s_{x_1} \\ a^1_{21}\,u^s_1 + a^1_{22}\,v^s_1 + a^1_{23}\,w^s_1 + a^1_{24}\,w^s_{1,x} &= N^s_{xy_1} \\ a^1_{31}\,u^s_1 + a^1_{32}\,v^s_1 + a^1_{33}\,w^s_1 + a^1_{34}\,w^s_{1,x} &= H^s_1 \\ a^1_{41}\,u^s_1 + a^1_{42}\,v^s_1 + a^1_{43}\,w^s_1 + a^1_{44}\,w^s_{1,x} &= M^s_{x_1} \end{aligned} \tag{17}$$

and

$$\begin{aligned} a^2_{11}\,u^s_2 + a^2_{12}\,v^s_2 &= N^s_{x_2} \\ a^2_{21}\,u^s_2 + a^2_{22}\,v^s_2 &= N^s_{xy_2} \end{aligned} \tag{18}$$

and the general elastic boundary conditions valid in the limit as $E_r \to \infty$ (fully clamped edges)

For n=0

$$\begin{aligned} b^o_{11}\,H^s_0 + b^o_{12}\,(M^s_{x_0} + \lambda\bar{q}) &= w^s_0 + W_\nu \\ b^o_{21}\,H^s_0 + b^o_{22}\,(M^s_{x_0} + \lambda\bar{q}) &= w^s_{0,x} \end{aligned} \tag{19}$$

For n≥2

$$\begin{aligned} b^1_{11}N^s_{x_1} + b^1_{12}\,N^s_{xy_1} + b^1_{13}\,H^s_1 + b^1_{14}\,M^s_{x_1} &= u^s_1 \\ b^1_{21}N^s_{x_1} + b^1_{22}\,N^s_{xy_1} + b^1_{23}\,H^s_1 + b^1_{24}\,M^s_{x_1} &= v^s_1 \\ b^1_{31}N^s_{x_1} + b^1_{32}\,N^s_{xy_1} + b^1_{33}\,H^s_1 + b^1_{34}\,M^s_{x_1} &= w^s_1 \\ b^1_{41}N^s_{x_1} + b^1_{42}\,N^s_{xy_1} + b^1_{43}\,H^s_1 + b^1_{44}\,M^s_{x_1} &= w^s_{1,x} \end{aligned} \tag{20}$$

and

$$b_{11}^2 N_{x_2}^s + b_{12}^2 N_{xy_2}^s = u_2^s$$
$$b_{21}^2 N_{x_2}^s + b_{22}^2 N_{xy_2}^s = v_2^s \tag{21}$$

The components of the boundary stiffness and of the boundary flexibility matrices are listed in Appendix A. Next these general elastic boundary conditions must be expressed in terms of the variables used in the shell analysis of Ref. [9], where the initial imperfection is given by

$$\bar{W} = t\, A_0(\bar{x}) + t\, A_1(\bar{x}) \cos n\theta \tag{22}$$

the radial displacement W and the Airy stress function F are assumed as

$$W = t\, W_v + t\, w_0(\bar{x}) + t\, w_1(\bar{x}) \cos n\theta$$
$$F = \frac{ERt^2}{c}\left\{-\frac{\lambda}{2}\theta^2 + f_0(\bar{x}) + f_1(\bar{x}) \cos n\theta + f_2(\bar{x}) \cos 2n\theta\right\} \tag{23}$$

and $\bar{x} = x/R$, $\theta = y/R$. This change of variables results in the following expressions

$$N_{x_1}^s = -n^2 f_1 \qquad N_{x_2}^s = -4n^2 f_2$$

$$N_{xy_1}^s = n f_1' \qquad N_{xy_2}^s = 2 n f_2'$$

$$H_0^s = -D_2\left\{w_0''' - \hat{B}_2 w_0' + \frac{1}{2}\hat{B}_3\left[(w_1 + 2A_1)w_1\right]' + \hat{B}_4\,\lambda(w_0' + A_0') + \hat{B}_5\left[f_1(w_1' + A_1') + f_1'(w_1 + A_1)\right]\right\}$$

$$H_1^s = -\bar{D}_{xx}\left\{w_1''' - \hat{B}_{15} w_1' + \hat{B}_{12} f_1''' + \hat{B}_{13} f_1' + \hat{B}_{23}\,\lambda\,(w_1' + A_1') + n^2 \hat{B}_{23}\left[(w_0' + A_0')f_1 + (w_1' + A_1')\,2f_2 + (w_1 + A_1)f_2'\right]\right\} \tag{24}$$

$$M_{x_0}^s = -D_2\left\{w_0'' - \hat{B}_2 w_0 + \hat{B}_6\,\lambda + \frac{1}{2}\hat{B}_3\,(w_1 + 2A_1)\,w_1\right\}$$

$$M_{x_1}^s = -\bar{D}_{xx}\left\{w_1'' - \hat{B}_{11} w_1 + \hat{B}_{12} f_1'' + \hat{B}_{13} f_1\right\}$$

further

$$
\begin{aligned}
u_1^s &= \frac{\bar{H}_{xx}}{cn^2}\left\{f_1''' - B_7 f_1' - B_8 w_1''' + B_9 w_1' - B_{10}(w_0' w_1 + w_0' A_1 + A_0' w_1)\right\} \\
u_2^s &= \frac{\bar{H}_{xx}}{4cn^2}\left\{f_2''' - 4B_7 f_2' - \tfrac{1}{2} B_{10}\,(w_1' w_1 + w_1' A_1 + A_1' w_1)\right\} \\
v_1^s &= \frac{\bar{H}_{xx}}{cn}\left\{f_1'' + B_{14} f_1 - B_8 w_1'' + B_9 w_1\right\} \\
v_2^s &= \frac{\bar{H}_{xx}}{2cn}\left\{f_2'' + 4B_{14} f_2 + \tfrac{1}{4} B_{10}\,(w_1 + 2A_1)\, w_1\right\}
\end{aligned}
\tag{25}
$$

where $(\,)' = d/d\bar{x}$ and the constants D_2, $\bar{D}_{xx}$, etc are listed in Appendix B. With the help of these expressions one can write the general elastic boundary conditions derived earlier in terms of the variables used in the shell analysis.

Introducing now the 16-dimensional vector variable $\underset{\sim}{Y}$ defined as

$$
\begin{aligned}
Y_1 &= f_1 \quad & Y_5 &= f_1' \quad & Y_9 &= f_1'' \quad & Y_{13} &= f_1''' \\
Y_2 &= f_2 \quad & Y_6 &= f_2' \quad & Y_{10} &= f_2'' \quad & Y_{14} &= f_2''' \\
Y_3 &= w_0 \quad & Y_7 &= w_0' \quad & Y_{11} &= w_0'' \quad & Y_{15} &= w_0''' \\
Y_4 &= w_1 \quad & Y_8 &= w_1' \quad & Y_{12} &= w_1'' \quad & Y_{16} &= w_1'''
\end{aligned}
\tag{26}
$$

then the system of governing equations and the general elastic boundary conditions can be reduced to the following nonlinear 2-point boundary value problem

$$
\begin{aligned}
&\frac{d}{d\bar{x}}\,\underset{\sim}{Y} = \underset{\sim}{f}\,(\bar{x},\ \underset{\sim}{Y};\ \lambda) \qquad \text{for } 0 \le \bar{x} \le \frac{L}{R} \\
&\underset{\sim}{g}\,(\bar{x} = 0,\ \underset{\sim}{Y}(0),\ \lambda) = 0 \qquad \text{at } \bar{x} = 0 \\
&\underset{\sim}{h}\,(\bar{x} = \frac{L}{R},\ \underset{\sim}{Y}(\frac{L}{R}),\ \lambda) = 0 \qquad \text{at } \bar{x} = \frac{L}{R}
\end{aligned}
\tag{27}
$$

where the general nonlinear boundary conditions are specified by the 8-dimensional vectors $\underset{\sim}{g}$ and $\underset{\sim}{h}$. The solution of this nonlinear 2-point boundary value problem will then locate the limit point of the prebuckling states. By

definition, the value of the loading parameter λ corresponding to the limit point will be the theoretical buckling load (see Fig. 8).

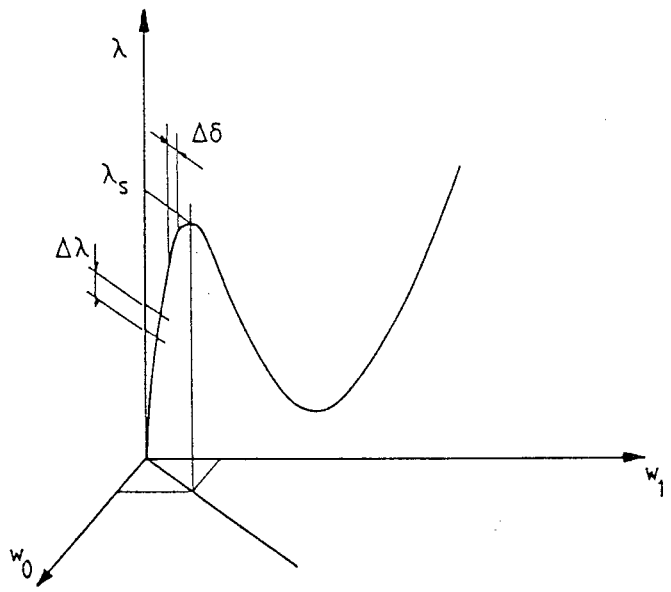

Fig. 8. Location of the limit point for an imperfect shell.

Using load increments $\Delta\lambda$ the solution fails to converge close to and beyond the limit point. However, if one switches to using increments in (say) 'end-shortening' $\Delta\delta$ then one is able to extend the response curve beyond the limit point.

NUMERICAL ANALYSIS

Due to the highly nonlinear nature of the above 2-point boundary value problem anything but a numerical solution is out of question. Due to the very satisfactory results obtained in Ref. [9] with the so-called 'Parallel Shooting Method' it was decided to modify it for the present problem. Though the code has been programmed to employ parallel shooting over 8 intervals, for the purpose of discribing the method let us consider just 'double shooting' or 'parallel shooting over 2 intervals'.

Initially let us associate the following 2 initial value problems with the above 2-point nonlinear boundary value problem

$$\frac{d}{d\bar{x}}\,\underset{\sim}{U} = \underset{\sim}{f}\,(\bar{x},\ \underset{\sim}{U};\ \lambda) \qquad \text{for } 0 \leq \bar{x} \leq \bar{x}_0 \qquad \underline{\text{Forward Integration}}$$

$$\underset{\sim}{U}(0) = \underset{\sim}{s} \tag{28}$$

and

$$\frac{d}{d\bar{x}} \underset{\sim}{V} = \underset{\sim}{f}\ (\bar{x},\ \underset{\sim}{V};\ \lambda) \qquad \text{for } \bar{x}_0 \leq \bar{x} \leq \frac{L}{R} \qquad \underline{\text{Backward Integration}}$$

$$\underset{\sim}{V}\ (\tfrac{L}{R}) = \underset{\sim}{t} \tag{29}$$

where $\underset{\sim}{s} = \underset{\sim}{Y}\ (0)$ and $\underset{\sim}{t} = \underset{\sim}{Y}\ (\frac{L}{R})$ are 16-dimensional initial guess vectors. Under appropriate smoothness conditions on the nonlinear vector function $\underset{\sim}{f}\ (\bar{x},\ \underset{\sim}{y},\ \lambda)$ one is assured of the existence of unique solution of these initial value problems, here denoted by

$$\underset{\sim}{U}\ (\bar{x},\ \underset{\sim}{s},\ \lambda) \text{ and } \underset{\sim}{V}\ (\bar{x},\ \underset{\sim}{t},\ \lambda).$$

These solutions must satisfy matching conditions at $\bar{x} = \bar{x}_0$ (see also Fig. 9).

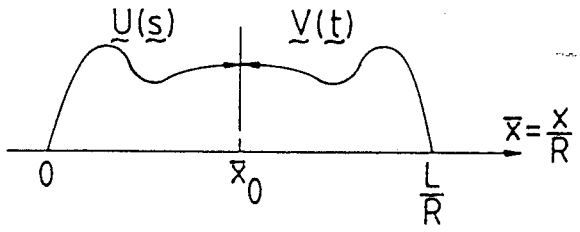

Fig. 9. Matching conditions at $\bar{x} = \bar{x}_0$.

Introducing the new vector function $\underset{\sim}{\varphi}$ the matching conditions at $\bar{x} = \bar{x}_0$ can be written as

$$\underset{\sim}{\varphi}\ (\underset{\sim}{S}) = \underset{\sim}{U}(\bar{x} = \bar{x}_0,\ \underset{\sim}{s},\ \lambda) - \underset{\sim}{V}\ (\bar{x} = \bar{x}_0,\ \underset{\sim}{t},\ \lambda) = 0 \tag{30}$$

where

$$\underset{\sim}{S} = \begin{pmatrix} \underset{\sim}{s} \\ \underset{\sim}{t} \end{pmatrix} \tag{31}$$

Thus the solution of the nonlinear 2-point boundary-value problem (27) has been transformed to the solution of the two associated initial value problems (28)-(29) and to the finding of the roots $\underset{\sim}{S}$ (a 32-dimensional vector) of the following system of simultaneous equations

$$\underset{\sim}{\Phi}(\underset{\sim}{S}) = \begin{bmatrix} \underset{\sim}{g}\ (\bar{x} = 0,\ \underset{\sim}{s},\ \lambda) \\ \underset{\sim}{\varphi}\ (\bar{x} = \bar{x}_0,\ \underset{\sim}{S},\ \lambda) \\ \underset{\sim}{h}\ (\bar{x} = \frac{L}{R},\ \underset{\sim}{t},\ \lambda) \end{bmatrix} = 0 \tag{32}$$

Using Newton's method for finding the roots of $\underset{\sim}{\Phi}(\underset{\sim}{S}) = 0$ one has the following iteration scheme

$$\underset{\sim}{S}^{\nu+1} = \underset{\sim}{S}^{\nu} + \Delta\underset{\sim}{S}^{\nu} \tag{33}$$

where $\Delta\underset{\sim}{S}^{\nu}$ is the solution of the 32nd-order linear algebraic system

$$\frac{\partial \underset{\sim}{\Phi}}{\partial \underset{\sim}{S}} (\underset{\sim}{S}^{\nu}) \, \Delta\underset{\sim}{S}^{\nu} = - \underset{\sim}{\Phi}(\underset{\sim}{S}^{\nu}) \tag{34}$$

To apply Newton's method one must be able to find the Jacobian J

$$J(\underset{\sim}{S}^{\nu}) = \frac{\partial \underset{\sim}{\Phi}}{\partial \underset{\sim}{S}} (\underset{\sim}{S}^{\nu}) = \begin{bmatrix} \frac{\partial g_1}{\partial S_1} & \cdots & \frac{\partial g_1}{\partial S_{16}} & 0 & \cdots & 0 \\ \cdots & & \cdots & \cdots & & \cdots \\ \frac{\partial g_8}{\partial S_1} & \cdots & \frac{\partial g_8}{\partial S_{16}} & 0 & \cdots & 0 \\ \frac{\partial \varphi_1}{\partial S_1} & \cdots & \frac{\partial \varphi_1}{\partial S_{16}} & \frac{\partial \varphi_1}{\partial S_{17}} & \cdots & \frac{\partial \varphi_1}{\partial S_{32}} \\ \cdots & & \cdots & \cdots & & \cdots \\ \cdots & & \cdots & \cdots & & \cdots \\ \frac{\partial \varphi_{16}}{\partial S_1} & \cdots & \frac{\partial \varphi_{16}}{\partial S_{16}} & \frac{\partial \varphi_{16}}{\partial S_{17}} & \cdots & \frac{\partial \varphi_{16}}{\partial S_{32}} \\ 0 & \cdots & 0 & \frac{\partial h_1}{\partial S_{17}} & \cdots & \frac{\partial h_1}{\partial S_{32}} \\ \cdots & & \cdots & \cdots & & \cdots \\ 0 & \cdots & 0 & \frac{\partial h_8}{\partial S_{17}} & \cdots & \frac{\partial h_8}{\partial S_{32}} \end{bmatrix} \tag{35}$$

Notice that the components of this Jacobian involving derivatives of the components of the specified boundary vectors $\underset{\sim}{g}$ anf $\underset{\sim}{h}$ can be calculated analytically. However, the components involving derivatives of the matching conditions must be obtained by solving the appropriate variational equations. In order to solve for these components let us introduce the following new vectors

$$\underset{\sim}{W}_i = \frac{\partial \underset{\sim}{U}}{\partial S_i} \text{ for } i = 1,2,\ldots,16$$

and (36)

$$\underset{\sim}{Z}_i = \frac{\partial \underset{\sim}{V}}{\partial S_i} \text{ for } i = 17,18,\ldots,32$$

which are the solutions of the corresponding variational equations obtained by implicit differentiation of the associated initial value problems. Thus for i=1,2,...,16 one must solve

$$\frac{d}{d\bar{x}}\,\underset{\sim}{W}_i = \frac{\partial \underset{\sim}{f}}{\partial \underset{\sim}{U}}\,(\bar{x},\ \underset{\sim}{U},\ \lambda)\ \underset{\sim}{W}_i \quad \text{for } 0 \le \bar{x} \le \bar{x}_0 \quad \underline{\text{Forward Integration}}$$

$$\underset{\sim}{W}_i(0) = \underset{\sim}{I}_i \tag{37}$$

and for i = 17,18,...,32

$$\frac{d}{d\bar{x}}\,\underset{\sim}{Z}_i = \frac{\partial \underset{\sim}{f}}{\partial \underset{\sim}{V}}\,(\bar{x},\ \underset{\sim}{V},\ \lambda)\ \underset{\sim}{Z}_i \quad \text{for } \bar{x}_0 \le \bar{x} \le \frac{L}{R} \quad \underline{\text{Backward Integration}}$$

$$\underset{\sim}{Z}_i\left(\frac{L}{R}\right) = \underset{\sim}{I}_i \tag{38}$$

where $\underset{\sim}{I}_i = [0,\ldots,0,1,0,\ldots,0]^T$ is the ith-unit vector in the n-space. Notice that now the components of the Jacobian matrix J'

$$J' = \frac{\partial \underset{\sim}{f}}{\partial \underset{\sim}{U}}\,(\bar{x},\ \underset{\sim}{U};\ \lambda) = \frac{\partial \underset{\sim}{f}}{\partial \underset{\sim}{V}}\,(\bar{x},\ \underset{\sim}{V};\ \lambda) = \begin{bmatrix} \frac{\partial f_1}{\partial U_1} & \frac{\partial f_1}{\partial U_2} & \cdots & \frac{\partial f_1}{\partial U_{16}} \\ \frac{\partial f_2}{\partial U_1} & \cdots & & \\ \cdots & & & \\ \frac{\partial f_{16}}{\partial U_1} & \cdots & \cdots & \frac{\partial f_{16}}{\partial U_{16}} \end{bmatrix} \tag{39}$$

can be calculated analytically.

Since the Jacobian J' is a function of $\underset{\sim}{U}$ (or $\underset{\sim}{V}$), therefore the variational equations (37) depend step-by-step on the results of the associated initial value problem (28) and the variational equations (38) depend step-by-step on the results of the associated initial value problem (29). Thus the variational equations depend on the initial guess $\underset{\sim}{S}^{\nu}$. Also, it is advantageous to integrate the 16 variational equations simultaneously with the corresponding associated initial value problem. This results, for double shooting, in a 272 dimensional, 1st-order, nonlinear differential equation.

Since in the case of an axially compressed imperfect cylindrical shell the nonlinear solution approaches the linearized solution asymptotically as $\lambda \to 0$, therefore for sufficiently low values of the axial load parameter λ one can use the linearized solutions as starting values for the nonlinear iteration scheme.

Solutions of the linearized problem are also obtained by the shooting method. It has been shown in the literature [12] that for the linearized 2-point boundary value problem Newton's method yields the correct initial vector $\underline{S}$ directly without the need of iterations. The solution of the associated initial value problems and of the variational equations was done by the library subroutine DEQ from Caltech's Willis Booth Computing Center. DEQ uses the method of Runge-Kutta-Gill to compute starting values for an Adams-Moulton corrector-predictor scheme. The program includes an option with variable interval size and uses automatic truncation error control.

NUMERICAL RESULTS

To investigate the effect of elastic boundary conditions initially the perfect stringer stiffened shell AS-2 has been analyzed. The elastic boundary conditions were modeled by symmetrically placed symmetrical rings of square cross-section. Following an idea by Almroth [5] the ring area is set equal to Ct^2 where C is a number and t is the wall thickness of the shell (see Fig. 10). The general elastic boundary conditions in the limit as $E_r \to \infty$ (Eqs. 19-21) reduce in this case to

For n=0

$$b_{11}^0 H_0^s = w_o^s + W_\nu$$
$$b_{22}^0 (M_{x_0}^s + \lambda \bar{q}) = w_{0,x}^s \qquad (40)$$

For n≥2

$$b_{11}^1 N_{x_1}^s + b_{14}^1 M_{x_1}^s = u_1^s$$
$$b_{22}^1 N_{xy_1}^s + b_{23}^1 H_1^s = v_1^s$$
$$b_{32}^1 N_{xy_1}^s + b_{33}^1 H_1^s = w_1^s \qquad (41)$$
$$b_{41}^1 N_{x_1}^s + b_{44}^1 M_{x_1}^s = w_{1,x}^s$$

and

$$b_{11}^2 N_{x_2}^s = u_2^s$$
$$b_{22}^2 N_{xy_2}^s = v_2^s \qquad (42)$$

It is interesting that even for this symmetrical case the stiffness matrix of the ring does not reduce to a diagonal matrix. Thus using a diagonal matrix to model ring supported elastic boundary conditions may lead to serious inaccuracies in the predicted critical load and buckling mode as has been pointed out in Ref. [13].

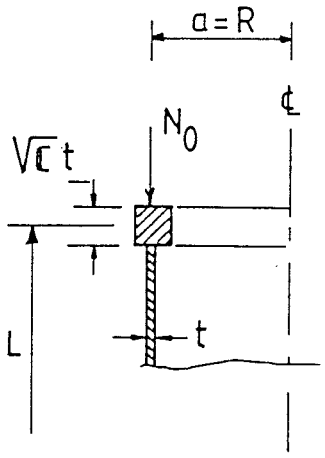

Fig. 10. Symmetrically placed symmetrical end-ring.

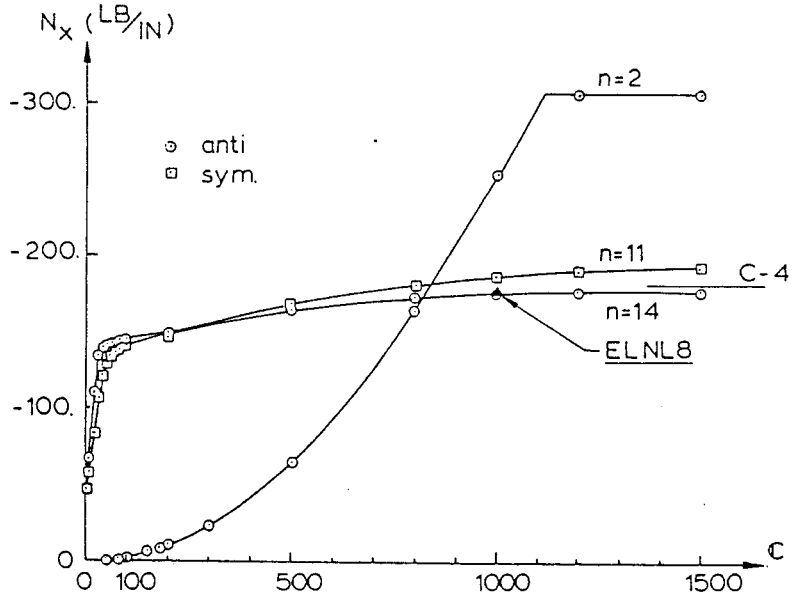

Fig. 11. Critical loads for shell AS-2 with elastic end rings.

Varying the size of the end-rings one can calculate the critical buckling loads of the perfect stringer stiffened shell AS-2 supported by elastic end-rings yielding the results shown in Fig. 11. The properties of the shell AS-2 are listed in Table 1.

Looking now at the buckling mode shapes corresponding to the 3 curves shown in Fig. 11, the variation of the antisymmetric mode shapes with n (the number

of full waves in the circumferential direction) for C=500 is displayed in Fig. 12. Notice that for n=2 the large deformation of the end-ring leads to the inextensional buckling mode at a relatively low buckling load.

Variation of the antisymmetrical mode shapes with the ring size parameter C for n=14 is shown in Fig. 13. Whereas Fig. 14 displays the variation of the symmetrical mode shapes with the ring size parameter C for n=11. Notice that in both cases weak end-rings result in edge buckling at relatively low buckling loads.

Returning to the results plotted in Fig. 11 it is clear that there is a critical size of the end-ring below which the ring strain energy controls the buckling and the buckling mode is inextensional. This phenomena is governed by Cohen's critical threshold parameter [14]

$$\Lambda_c = \left[\frac{(EI_x)^r}{(D\ L/2)^s}\right]^* \approx 100 \tag{43}$$

where I_x is the moment of inertia of the ring cross-section and for stringer stiffened shells

$$D = \frac{Et^3}{12(1-\nu^2)} + \frac{E(I_s+A_s e_s^2)}{d_s} \quad (= C_{44}) \tag{44}$$

the bending stiffness of the shell wall plus stringer combination.

All the buckling load calculations for the 3 curves shown in Fig. 11 were done with the SRA [10] computer code with the exception of the point labeled ELNL8. This point was computed with the program described in this paper. As can be seen from Fig. 15 for vanishingly small initial imperfections the 2 separate branches of the response curve clearly define the location of the bifurcation point. The accuracy of this approach is quite satisfactory.

Table 1. Geometric and material properties of shell AS-2.

t	$= 1.96596 \times 10^{-2}$	cm	$(= 0.00774$	IN)
L	$= 13.97$	cm	$(= 5.5$	IN)
R	$= 10.16$	cm	$(= 4.0$	IN)
d_1	$= 8.03402 \times 10^{-1}$	cm	$(= 0.3161$	IN)
e_1	$= 3.36804 \times 10^{-2}$	cm	$(= 0.01326$	IN)
A_1	$= 7.98708 \times 10^{-3}$	cm^2	$(= 0.1238 \times 10^{-2}$	IN^2)
I_{11}	$= 1.50384 \times 10^{-6}$	cm^4	$(= 0.3613 \times 10^{-7}$	IN^4)
I_{t_1}	$= 4.94483 \times 10^{-6}$	cm^4	$(= 0.1188 \times 10^{-6}$	IN^4)
E	$= 6.89472 \times 10^{6}$	N/cm^2	$(= 10.10^6$	PSI)
ν	$= 0.3$			

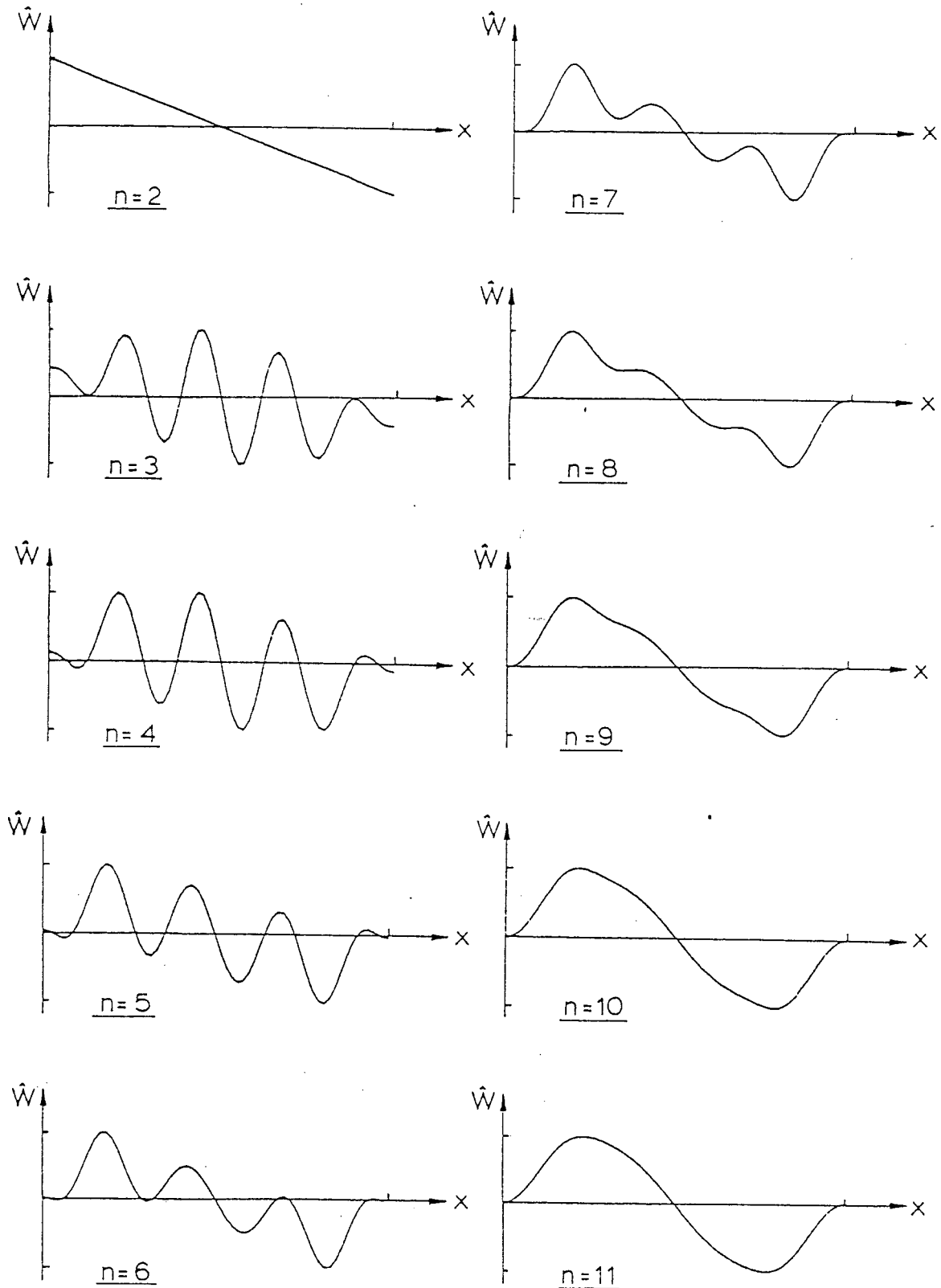

Fig. 12. Variation of anti-symmetric mode shapes with n for C=500.

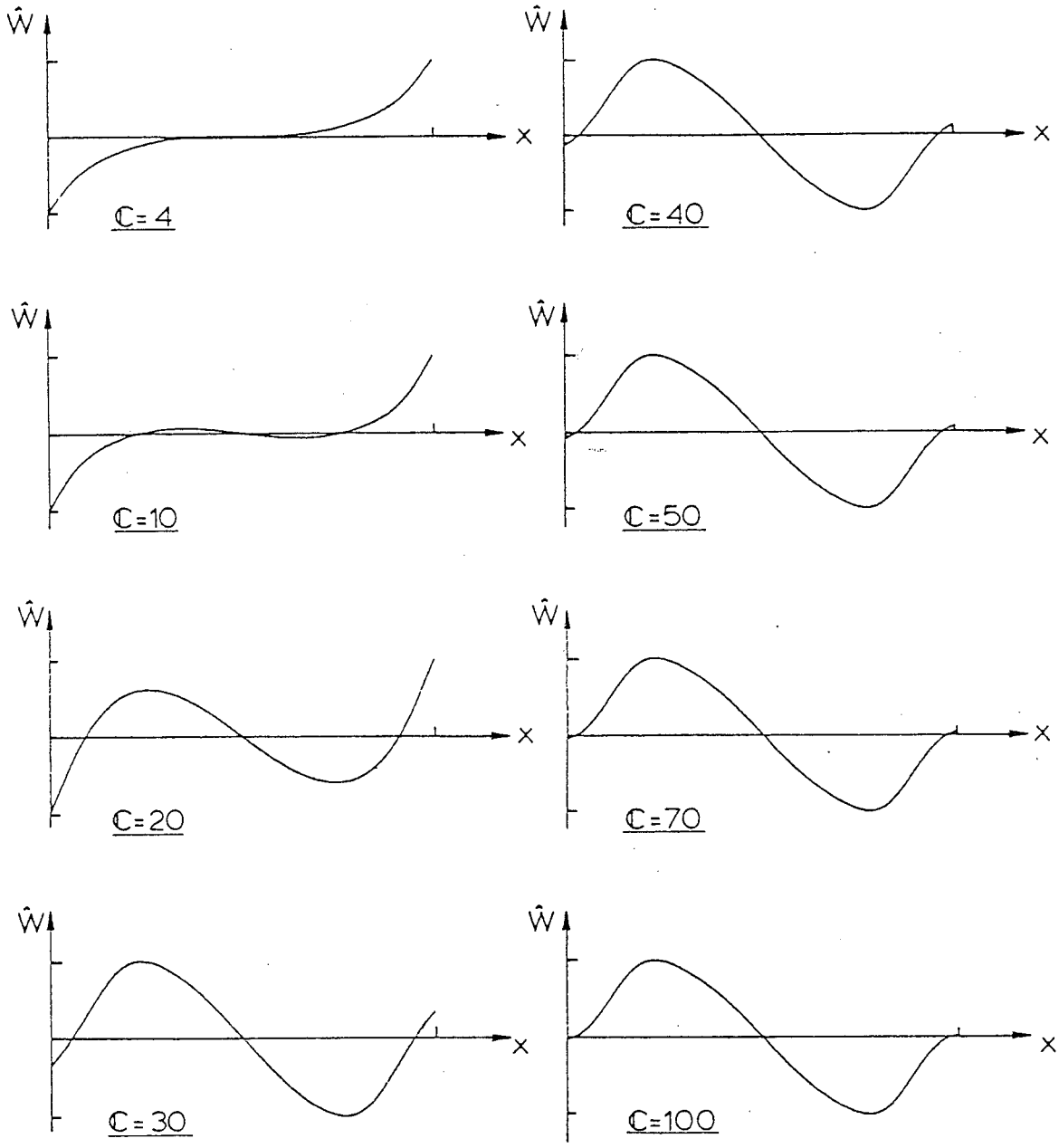

Fig. 13. Variation of anti-symmetric mode shapes with the ring size-parameter C (n=14).

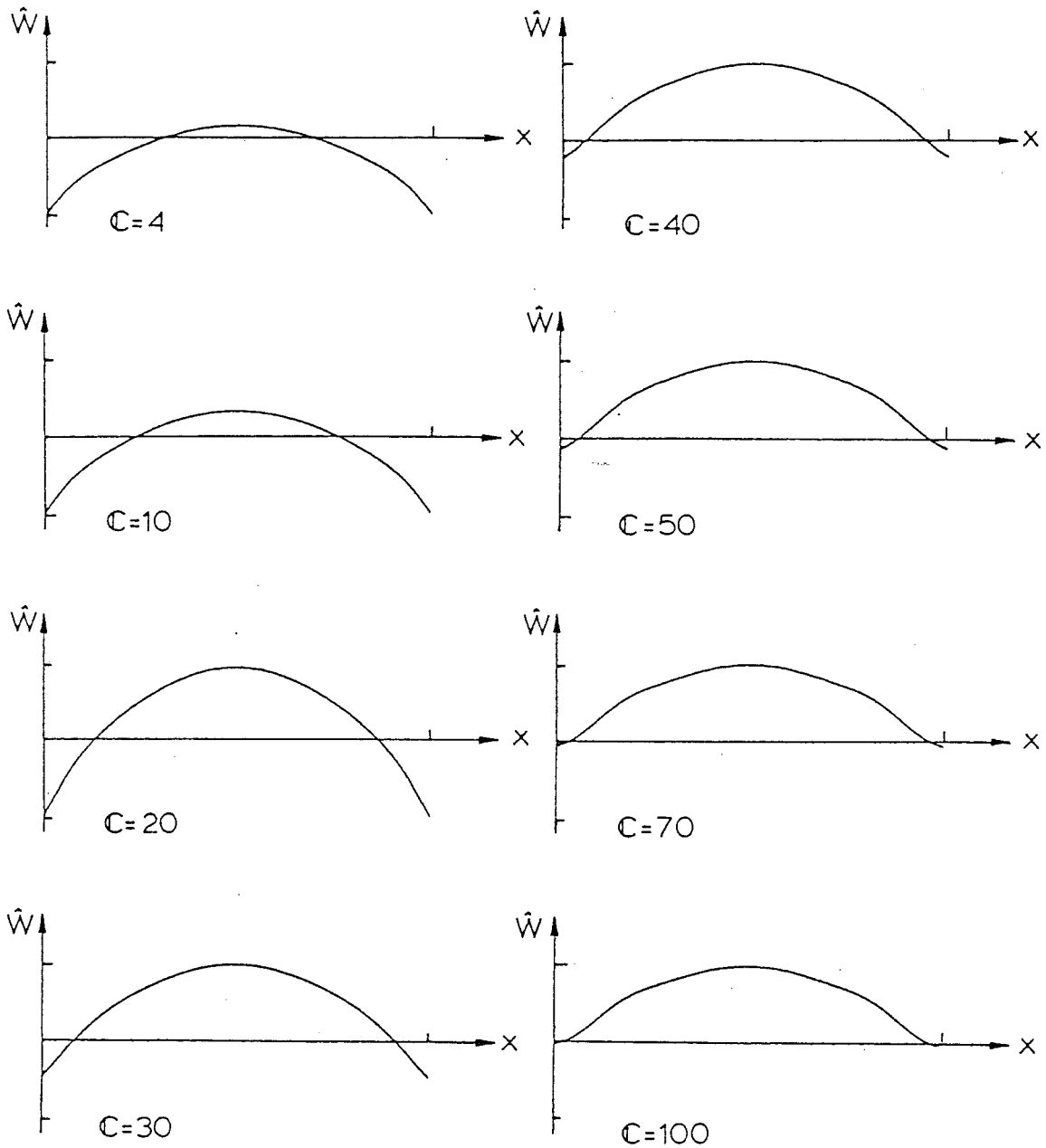

Fig. 14. Variation of symmetrical mode shapes with the ring size-parameter C (n=11).

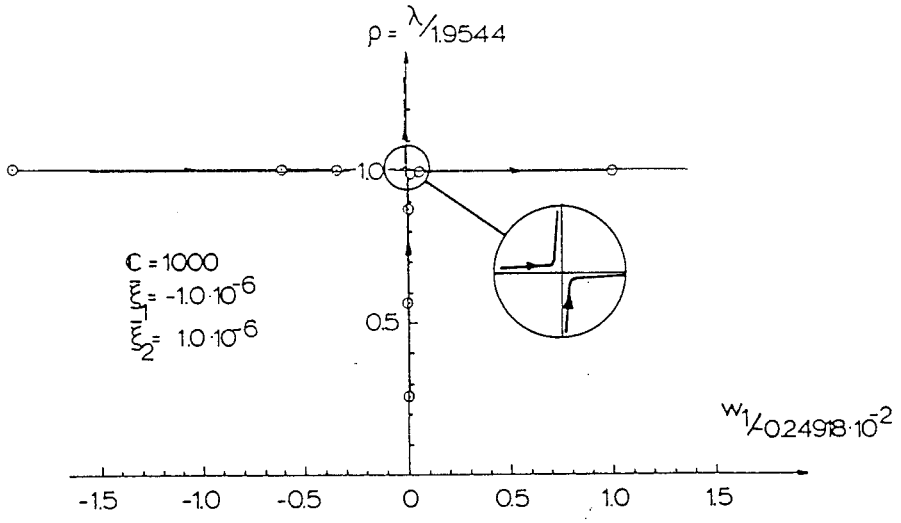

Fig. 15. Response paths for vanishingly small imperfections.

Finally the effect of varying the size of the end-rings while keeping the initial imperfections constant is investigated. Using the following imperfection

$$\frac{\bar{w}}{t} = -0.01 \cos \frac{2\pi x}{L} + 0.50 \sin \frac{\pi x}{L} \cos \frac{11 y}{R} \qquad (45)$$

the calculated buckling loads are tabulated in Table 2 for various size end-rings.

Table 2. Calculated buckling loads (n=11, symmetric).

C	PERFECT N_{BIF} (N/cm)	IMPERFECT N_s (N/cm)	$\rho_s = N_s / N_{BIF}$
50	- 226.406	- 165.568	0.731
100	- 246.460	- 174.520	0.708
500	- 292,408	- 195.236	0.668
1000	- 328.610	- 215.841	0.657
C-4	- 358.607	- 238.868	0.666

C-4: $u = v = w = w_{,x} = 0$

From these results it is evident that increasing the sizes of the end-rings produces an increase of the buckling loads. That the shells with weak end-rings appear to be less imperfection sensitive has a simple explanation. It is well known that imperfections affine to the buckling mode produce the largest decrease in the buckling load. However, since weak end rings result in edge-buckling whereas the initial imperfection used (see Eq. 21) consists of trigonometric functions, therefore in these cases the initial imperfections and the buckling modes are not affine, hence they are less damaging.

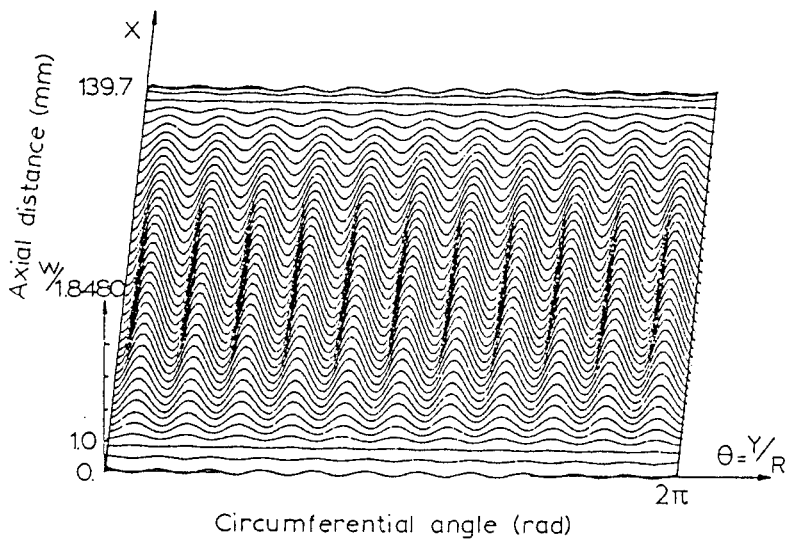

Fig. 16. Calculated prebuckling growth of the stringer stiffened shell AS-2 at λ_s=1.0430
(Boundary conditions: symmetrical end rings - C=50).

Figures 16 and 17 display the calculated prebuckling growth at the limit point for a weak end-ring (C=50) and a strong end-ring (C=1000). Notice that besides increasing the buckling load a stronger end-ring reduces the maximum normal displacement at the limit point.

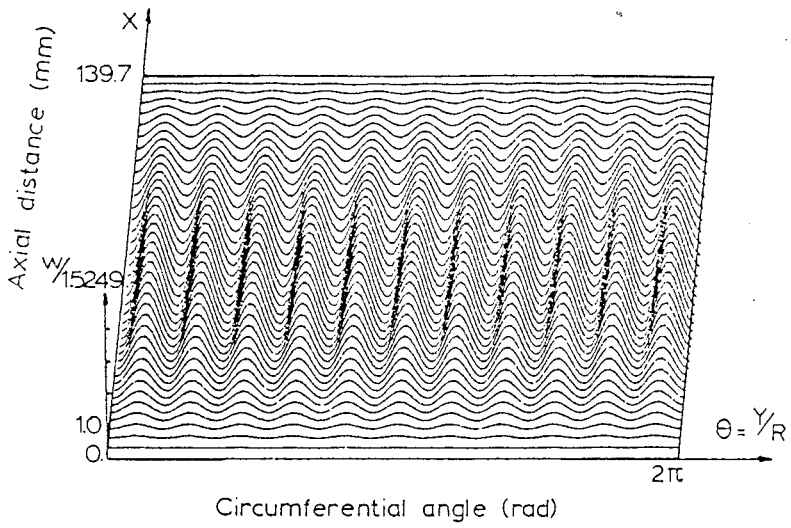

Fig. 17. Calculated prebuckling growth of the stringer stiffened shell AS-2 at λ_s=1.3597
(Boundary conditions: symmetrical end rings - C=1000).

CONCLUSIONS

The results obtained sofar clearly indicate that there exists a critical threshold parameter, consisting of the ratio of the in-plane ring bending stiffness and the bending stiffness of the shell wall-stringer combination, which governs the buckling behaviour of axially compressed stringer stiffened shells with elastic edge supports.

If the end-rings are weaker than the critical value of the threshold parameter then the ring strain energy controls the buckling and the buckling mode tends to be inextensional. That is the end-rings deform and the shell generators remain essentially straight.

If, however, the rigidity of the end-rings exceeds the critical value of the threshold parameter then the ring strain energy is negligible and the buckling mode tends to be sinusoidal. That is, the end-rings remain essentially undeformed.

Finally, as a continuation of the present work it appears necessary to investigate the interaction between the dominant initial imperfection of the shell body with n full waves in the circumferential direction and an imperfect end-ring with n_R full waves in the circumferential direction. It is hoped that this addition will make a more reliable modeling of the actual experimental boundary conditions possible.

ACKNOWLEDGEMENT

The authors wish to express their sincere thanks to Mrs. Irma Eggens for the skilful typing of the manuscript. The fine artwork by Mr. J. de Vries is also very much appreciated. This paper has been presented at the XVIth IUTAM Congress in Lyngby, Denmark, August, 1984.

REFERENCES

1. Koiter, W.T.: 'On the Stability of Elastic Equilibrium', Ph.D. Thesis 1945, in Dutch, TU-Delft, The Netherlands, H.T. Paris, Amsterdam. (English translation issued as NASA TT F-10, 833 p., 1967.)
2. Budiansky, B. and Hutchinson, J.W.: 'Dynamic Buckling of Imperfection Sensitive Structures', In: Proceedings 11th IUTAM Congress, pp. 636-51, 1964, Springer Verlag, Berlin.
3. Singer, J. and Rosen, A.: 'The Influence of Boundary Conditions on the Buckling of Stiffened Cylindrical Shells', In: Proceedings IUTAM Symposium Buckling of Structures, Harvard University Cambridge, Mass., June 1974, B. Budiansky (ed.), pp. 227-50, Spinger Verlag, Berlin, 1976.
4. Hoff, N.J.: 'Buckling of Thin Shells', In: Proceedings of an Aerospace Symposium of Distinguished Lectures in Honor of Theodore Von Karman on his 80th Anniversary', 1961, pp. 1-42, Institute of Aerospace Sciences, New York.
5. Almroth, B.O.: 'Influence of Imperfections and Edge Constraint on the Buckling of Axially Compressed Cylinders', NASA, CR-432, April 1966.
6. Arbocz, J.: 'Collapse Load Calculations for Axially Compressed Imperfect Stringer Stiffened Shells', Paper AIAA-84-0888 in Proc. AIAA/ASME/ASCE/AHS 25th Structures, Structural Dynamics and Materials Conference, May 14-16, 1984, Palm Springs, California, pp. 130-139.
7. Singer, J. Arbocz, J. and Babcock, C.D. In: 'Buckling of Imperfect Stiffened Cylindrical Shells under Axial Compression', AIAA Journal, 9(1), January 1971, pp. 68-75.
8. Almroth, B.O., Brogan, F.A., Miller, E., Zele, F. and Peterson, H.T.: 'Collapse Analysis for Shells of General Shapes', II User's Manual for the STAGS-A Computer Code, Air Force Flight Dynamics Lab., Wright Patterson AFB, AFFDL-TR-71-8.
9. Arbocz, J. and Sechler, E.E.: 'On the Buckling of Stiffened Imperfect Cylindrical Shells', AIAA Journal, 15(11), November 1976, pp. 1611-17.
10. Cohen, G.A.: 'Computer Analysis of Ring-Stiffened Shells of Revolution', NASA, CR-2085, 1973.
11. Arbocz, J., Vermeulen, P.G. and Van Geer, J.: 'On the Buckling of Axially Compressed Imperfect Orthotropic Shells with Elastic Edge Supports', Report LR-540, Aeronautics Faculty, TU-Delft, The Netherlands, March 1988.
12. Keller, H.: 'Numerical Methods for Two-Point Boundary Value Problems', Blaisdell Publishing Co., Waltham, Mass., 1968.
13. Dixon, S.C., Weeks, G.E. and Anderson, M.S.: 'Effect of Edge Restraint Coupling on Buckling of Ring-Supported Cylinders', AIAA Journal, 6(8), August 1968, pp. 1602-04.
14. Cohen, G.A.: 'Buckling of Axially Compressed Cylindrical Shells with Ring-Stiffened Edges', AIAA Journal, 4(10), October 1966, pp. 1859-62.
15. Arbocz, J.: 'The Effect of Initial Imperfections on shell stability'. In: Thin-Shell Structures. Edited by Y.C. Fung, E.E. Sechler. Prentice-Hall, 1974.

Appendix A The boundary stiffness and boundary flexibility matrices

The components of the boundary stiffness matrices in Eqs. (16), (17) and (18) are respectively

for n=0

$$a^0_{11} = \left(\frac{R}{a}\right)^2 \bar{D}_{11} \qquad a^0_{12} = \left(\frac{R}{a}\right)^2 \bar{D}_{12}$$

$$a^0_{21} = -\left(\frac{R}{a}\right)^2 \bar{D}_{12} \qquad a^0_{22} = -\left[\bar{D}_{22} + \left(\frac{R}{a}\right)^2 \frac{e_x}{R} \bar{D}_{12}\right]$$

for n ≥ 2

$$a^1_{14} = \frac{1}{4c} \left(\frac{t}{a}\right)^2 n^2 \bar{D}_{33} \qquad a^1_{12} = \frac{-1}{4c} \left(\frac{t}{a}\right)^2 n^3 \frac{a}{R} \bar{D}_{34}$$

$$a^1_{21} = \frac{1}{4c} \left(\frac{t}{a}\right)^2 n^3 \bar{D}_{43} \qquad a^1_{22} = \frac{1}{4c} \left(\frac{t}{a}\right)^2 n^2 \frac{a}{R} \bar{D}_{44}$$

$$a^1_{31} = \left(\frac{R}{a}\right)^2 n^2 \bar{D}_{53} \qquad a^1_{32} = -\left(\frac{R}{a}\right)^2 n \frac{a}{R} \bar{D}_{54}$$

$$a^1_{41} = \left(\frac{R}{a}\right) n^2 \left(\bar{D}_{63} + \frac{e_z}{a} \bar{D}_{33} - \frac{e_x}{a} \bar{D}_{53}\right)$$

$$a^1_{42} = \left(\frac{R}{a}\right) n \left(\frac{-a}{R} \bar{D}_{64} - n^2 \frac{e_z}{R} \bar{D}_{34} + \frac{e_z}{R} \bar{D}_{54}\right)$$

$$a^1_{13} = \frac{1}{4c} \left(\frac{t}{a}\right)^2 n^4 \bar{D}_{35} \qquad a^1_{14} = \frac{1}{4c} \left(\frac{t}{a}\right)^2 n^2 \bar{D}_{36}$$

$$a^1_{23} = \frac{-1}{4c} \left(\frac{t}{a}\right)^2 n \bar{D}_{45} \qquad a^1_{24} = \frac{1}{4c} \left(\frac{t}{a}\right)^2 n \bar{D}_{46}$$

$$a^1_{33} = \left(\frac{R}{a}\right)^2 \bar{D}_{55} \qquad a^1_{34} = \left(\frac{R}{a}\right)^2 \bar{D}_{56}$$

$$a^1_{43} = \left(\frac{R}{a}\right)\left(n^2 \bar{D}_{65} + n^4 \frac{e_z}{a} \bar{D}_{35} - \frac{e_x}{a} \bar{D}_{55}\right)$$

$$a^1_{44} = \left(\frac{R}{a}\right)\left(\bar{D}_{66} + n^2 \frac{e_z}{a} \bar{D}_{36} - \frac{e_x}{a} \bar{D}_{56}\right)$$

and

$$a^2_{11} = \left(\frac{t}{a}\right)^2 \frac{n^2}{c} \bar{D}_{77} \qquad a^2_{12} = -2\left(\frac{a}{R}\right)\left(\frac{t}{a}\right)^2 \frac{n^3}{c} \bar{D}_{78}$$

$$a^2_{21} = 2\left(\frac{t}{a}\right)^2 \frac{n^3}{c} \bar{D}_{87} \qquad a^2_{22} = \left(\frac{a}{R}\right)\left(\frac{t}{a}\right)^2 \frac{n^2}{c} \bar{D}_{88}$$

where the stiffness coefficients $\bar{D}_{ij}$ are

$$\bar{D}_{11} = \frac{a^2 EA}{aD} \qquad \left(\text{where } D = \frac{Et^3}{4c^2}\right)$$

$$\bar{D}_{12} = \left(\frac{a^2 EA}{aD}\right) \frac{e_x}{R}$$

$$\bar{D}_{22} = \frac{EI_z}{aD}$$

$$\bar{D}_{33} = n^2 \left[\left(\frac{EI_z}{aD}\right) - \frac{e_x}{R}\left(\frac{EI_{xz}}{aD}\right)\right] + \left(\frac{GJ}{aD}\right)$$

$$\bar{D}_{34} = \left(\frac{EI_{xz}}{aD}\right)$$

$$\bar{D}_{35} = \left(\frac{EI_{xz}}{aD}\right)\left(1 - \frac{e_z}{R}\right)$$

$$\bar{D}_{36} = n^2\left(\frac{EI_{xz}}{aD}\right)\frac{e_x}{R} - \left(\frac{EI_z}{aD}\right)\left(\frac{a}{R} + n^2\frac{e_z}{R}\right) - \left(\frac{GJ}{aD}\right)\left(\frac{a}{R} + \frac{e_z}{R}\right)$$

$$\bar{D}_{43} = \left[\left(\frac{EI_x}{aD}\right) + \left(\frac{a^2EA}{aD}\right)\right]\frac{e_x}{R} - \left(\frac{EI_{xz}}{aD}\right)$$

$$\bar{D}_{44} = \left[\left(\frac{EI_x}{aD}\right) + \left(\frac{a^2EA}{aD}\right)\right]$$

$$\bar{D}_{45} = \left[n^2\left(\frac{EI_x}{aD}\right)\left(1 - \frac{e_z}{R}\right) + \left(\frac{a^2EA}{aD}\right)\left(1 - n^2\frac{e_z}{R}\right)\right]$$

$$\bar{D}_{46} = \left(\frac{EI_{xz}}{aD}\right)\left(\frac{a}{R} + n^2\frac{e_z}{R}\right) - \left[n^2\left(\frac{EI_x}{aD}\right) + \left(\frac{a^2EA}{aD}\right)\right]\frac{e_x}{R}$$

$$\bar{D}_{53} = n^2\left[\left(\frac{EI_{xz}}{aD}\right) - \frac{e_x}{R}\left(\frac{EI_x}{aD}\right)\right] - \frac{e_x}{R}\left(\frac{a^2EA}{aD}\right)$$

$$\bar{D}_{54} = \left[n^2\left(\frac{EI_x}{aD}\right) + \left(\frac{a^2EA}{aD}\right)\right]$$

$$\bar{D}_{55} = n^4\left(\frac{EI_x}{aD}\right)\left(1 - \frac{e_z}{R}\right) + \left(\frac{a^2EA}{aD}\right)\left(1 - n^2\frac{e_z}{R}\right)$$

$$\bar{D}_{56} = \frac{e_x}{R}\left[n^4\left(\frac{EI_x}{aD}\right) + \left(\frac{a^2EA}{aD}\right)\right] - n^2\left(\frac{EI_{xz}}{aD}\right)\left(\frac{a}{R} + n^2\frac{e_z}{R}\right)$$

$$\bar{D}_{63} = \left(\frac{EI_z}{aD}\right) + \left(\frac{GJ}{aD}\right) - \frac{e_x}{R}\left(\frac{EI_{xz}}{aD}\right)$$

$$\bar{D}_{64} = \left(\frac{EI_{xz}}{aD}\right)$$

$$\bar{D}_{65} = \left(\frac{EI_{xz}}{aD}\right)\left(1 - \frac{e_z}{R}\right)$$

$$\bar{D}_{66} = n^2\left(\frac{EI_{xz}}{aD}\right)\frac{e_x}{R} - \left(\frac{EI_z}{aD}\right)\left(\frac{a}{R} + n^2\frac{e_z}{R}\right) - n^2\left(\frac{GJ}{aD}\right)\left(\frac{a}{R} + \frac{e_z}{R}\right)$$

$$\bar{D}_{77} = 4n^2\left[\left(\frac{EI_z}{aD}\right) - \frac{e_x}{R}\left(\frac{EI_{xz}}{aD}\right)\right] + \left(\frac{GJ}{aD}\right)$$

$$\bar{D}_{78} = \frac{EI_{xz}}{aD}$$

$$\bar{D}_{87} = \left[\left(\frac{EI_x}{aD}\right) + \frac{a^2EA}{aD}\right]\frac{e_x}{R} - \left(\frac{EI_{xz}}{aD}\right)$$

$$\bar{D}_{88} = \left(\frac{EI_x}{aD}\right) + \left(\frac{a^2EA}{aD}\right)$$

and the load parameter is

$$\lambda = N_o^r \Big/ \frac{Et^2}{cR} \qquad\qquad \bar{q} = 4c\,\frac{R}{t^2}q$$

Writing eq.(16) in matrix form the inversion can be done easily in closed form yielding eq.(19), where the components of the flexibility matrix are

<u>for n = 0</u>

$$b_{11}^0 = \left[\left(\frac{a}{R}\right)^2\frac{1}{\bar{D}_{11}} + \left(\frac{e_x}{R}\right)^2\frac{1}{\bar{D}_{22}}\right] \qquad b_{12}^0 = \frac{e_x}{R}\frac{1}{\bar{D}_{22}}$$

$$b_{21}^0 = -\left(\frac{e_x}{R}\right)\frac{1}{\bar{D}_{22}} \qquad b_{22}^0 = -\frac{1}{\bar{D}_{22}}$$

Writing eq.(17) in matrix form the inversion cannot be done easily in closed form.
The inversion will be done numerically in the computerprogram. So in general the components of the flexibility matrix will not be written out explicitly as in eq. (20) for $n \geq 2$

Finally, writing eq. (18) in matrix form the inversion can be done once again easily in closed form yielding eq. (21), where the components of the flexibility matrix are

<u>for $n \geq 2$</u>

$$b_{11}^2 = \left(\frac{a}{t}\right)^2 \frac{c}{n^2} \frac{\bar{D}_{88}}{(\bar{D}_{77}\,\bar{D}_{88} + 4n^2\,\bar{D}_{78}\,\bar{D}_{87})}$$

$$b_{12}^2 = 2\left(\frac{a}{t}\right)^2 \frac{c}{n} \frac{\bar{D}_{78}}{(\bar{D}_{77}\,\bar{D}_{88} + 4n^2\,\bar{D}_{78}\,\bar{D}_{87})}$$

$$b_{21}^2 = -2\left(\frac{R}{a}\right)\left(\frac{a}{t}\right)^2 \frac{c}{n} \frac{\bar{D}_{87}}{(\bar{D}_{77}\,\bar{D}_{88} + 4n^2\,\bar{D}_{78}\,\bar{D}_{87})}$$

$$b_{22}^2 = \left(\frac{R}{a}\right)\left(\frac{a}{t}\right)^2 \frac{c}{n^2} \frac{\bar{D}_{77}}{(\bar{D}_{77}\,\bar{D}_{88} + 4n^2\,\bar{D}_{78}\,\bar{D}_{87})}$$

In a special case, for a symmetrical ring with $e_x = e_z = I_{xz} = 0$ and $a = R$ these equations become considerably simpler. To start with the constants, the stiffness coefficients are now

$$\bar{D}_{11} = \frac{R^2 EA}{RD}$$

$$\bar{D}_{12} = 0 \qquad \bar{D}_{22} = \frac{EI_z}{RD}$$

$$\bar{D}_{33} = n^2 \left(\frac{EI_z}{RD}\right) + \left(\frac{GJ}{RD}\right) \qquad \bar{D}_{34} = 0$$

$$\bar{D}_{35} = 0 \qquad \bar{D}_{36} = -\left[\left(\frac{EI_z}{RD}\right) + \left(\frac{GJ}{RD}\right)\right]$$

$$\bar{D}_{43} = 0 \qquad \bar{D}_{44} = \left(\frac{EI_x}{RD}\right) + \left(\frac{R^2EA}{RD}\right)$$

$$\bar{D}_{45} = n^2\left(\frac{EI_x}{RD}\right) + \left(\frac{R^2EA}{RD}\right) \qquad \bar{D}_{46} = 0$$

$$\bar{D}_{53} = 0 \qquad \bar{D}_{54} = n^2\left(\frac{EI_x}{RD}\right) + \left(\frac{R^2EA}{RD}\right)$$

$$\bar{D}_{55} = n^4\left(\frac{EI_x}{RD}\right) + \left(\frac{R^2EA}{RD}\right) \qquad \bar{D}_{56} = 0$$

$$\bar{D}_{63} = \left(\frac{EI_z}{RD}\right) + \left(\frac{GJ}{RD}\right) \qquad \bar{D}_{64} = 0$$

$$\bar{D}_{65} = 0 \qquad \bar{D}_{66} = -\left[\left(\frac{EI_z}{RD}\right) + n^2\left(\frac{GJ}{RD}\right)\right]$$

$$\bar{D}_{77} = 4n^2 \left(\frac{EI_z}{RD}\right) + \left(\frac{GJ}{RD}\right) \qquad \bar{D}_{78} = 0$$

$$\bar{D}_{87} = 0 \qquad \bar{D}_{88} = \left(\frac{EI_x}{RD}\right) + \left(\frac{R^2EA}{RD}\right)$$

Now the components of the flexibility matrix in eq. (19) reduce to

for n=0

$$b^0_{11} = \frac{1}{\bar{D}_{11}} \qquad b^0_{12} = 0$$

$$b^0_{21} = 0 \qquad b^0_{22} = -\frac{1}{\bar{D}_{22}}$$

Writing eq. (17) in matrix form and putting in the $\bar{D}_{ij}$'s and zero's for the simple case of the symmetrical ring we arrive at

$$\begin{bmatrix} n^2 \bar{D}_{33} & 0 & 0 & n^2 \bar{D}_{36} \\ 0 & n^2 \bar{D}_{44} & -n \bar{D}_{45} & 0 \\ 0 & -n \bar{D}_{54} & \bar{D}_{55} & 0 \\ n^2 \bar{D}_{63} & 0 & 0 & \bar{D}_{66} \end{bmatrix} \begin{bmatrix} u^s_1 \\ v^s_1 \\ w^s_1 \\ w^s_{1,x} \end{bmatrix} = \begin{bmatrix} 4c \frac{R^2}{t^2} N^s_{x_1} \\ 4c \frac{R^2}{t^2} N^s_{xy_1} \\ H^s_1 \\ M^s_{x_1} \end{bmatrix}$$

It must be remarked here that also in the case of a symmetrical ring there are off-diagonal terms, so the first and the last equations and the second and the third equations remain coupled.
The inversion of the stiffness matrix into the flexibility matrix can now be done rather easily yielding eq. (20) where the components b_{ij} are explicitly

for n ≧ 2

$$b^1_{11} = \frac{4c R^2}{n^2 t^2} \frac{\bar{D}_{66}}{(\bar{D}_{33} \bar{D}_{66} - n^2 \bar{D}_{36} \bar{D}_{63})} \qquad b^1_{12} = 0$$

$$b^1_{21} = 0 \qquad b^1_{22} = \frac{4cR^2}{n^2t^2} \frac{\bar{D}_{55}}{(\bar{D}_{44}\,\bar{D}_{55} - \bar{D}_{45}\,\bar{D}_{54})}$$

$$b^1_{31} = 0 \qquad b^1_{32} = \frac{4cR^2}{nt^2} \frac{\bar{D}_{54}}{(\bar{D}_{44}\,\bar{D}_{55} - \bar{D}_{45}\,\bar{D}_{54})}$$

$$b^1_{41} = \frac{-\,4cR^2}{t^2} \frac{\bar{D}_{63}}{(\bar{D}_{33}\,\bar{D}_{66} - n^2\,\bar{D}_{36}\,\bar{D}_{63})} \qquad b^1_{42} = 0$$

$$b^1_{13} = 0 \qquad b^1_{14} = \frac{-\,\bar{D}_{36}}{(\bar{D}_{33}\,\bar{D}_{66} - n^2\,\bar{D}_{36}\,\bar{D}_{63})}$$

$$b^1_{23} = \frac{\bar{D}_{45}}{n\,(\bar{D}_{44}\,\bar{D}_{55} - \bar{D}_{45}\,\bar{D}_{54})} \qquad b^1_{24} = 0$$

$$b^1_{33} = \frac{\bar{D}_{44}}{(\bar{D}_{44}\,\bar{D}_{55} - \bar{D}_{45}\,\bar{D}_{54})} \qquad b^1_{34} = 0$$

$$b^1_{43} = 0 \qquad b^1_{44} = \frac{\bar{D}_{33}}{(\bar{D}_{33}\,\bar{D}_{66} - n^2\,\bar{D}_{36}\,\bar{D}_{63})}$$

and the components of eq. (21) reduce to

$$b^2_{11} = \frac{cR^2}{n^2t^2} \frac{1}{\bar{D}_{77}} \qquad b^2_{12} = 0$$

$$b_{21}^2 = 0 \qquad b_{22}^2 = \frac{cR^2}{n^2 t^2} \frac{1}{\bar{D}_{88}}$$

Appendix B

The coefficients in eqs. (24) and (25) are:

$$B_2 = 2c \frac{R \bar{Q}_{xx}}{t \bar{H}_{xx}} \qquad \hat{B}_2 = \frac{B_2}{D_2}$$

$$B_3 = cn^2 \frac{\bar{Q}_{xx}}{\bar{H}_{xx}} \qquad \hat{B}_3 = \frac{B_3}{D_2}$$

$$B_4 = 4c\frac{R}{t} \qquad \hat{B}_4 = \frac{B_4}{D_2}$$

$$B_5 = 2c \frac{R}{t} n^2 \qquad \hat{B}_5 = \frac{B_5}{D_2}$$

$$B_6 = 2\frac{R}{t} \bar{Q}_{xx} \frac{(1 + \mu_2)}{\nu} \qquad \hat{B}_6 = \frac{B_6}{D_2}$$

$$B_7 = \left[2 (1 + \nu) - \frac{\nu}{1+\mu_1} \bar{H}_{xx}\right] \frac{n^2}{\bar{H}_{xx}}$$

$$B_8 = \frac{t}{2R} \frac{\bar{Q}_{xx}}{\bar{H}_{xx}}$$

$$B_9 = \left[c - \frac{t}{2R} \frac{(1+\mu_1)}{\nu} \bar{Q}_{yy} n^2\right] \frac{1}{\bar{H}_{xx}}$$

$$B_{10} = c \frac{t n^2}{R \bar{H}_{xx}}$$

$$B_{11} = \nu (1 + \hat{\beta} \zeta_1 \chi_2) n^2 \qquad \hat{B}_{11} = \frac{B_{11}}{\bar{D}_{xx}}$$

$$B_{12} = 2 \frac{R}{t} \bar{Q}_{xx} \qquad \hat{B}_{12} = \frac{B_{12}}{\bar{D}_{xx}}$$

$$B_{13} = 2\frac{R}{t} \bar{Q}_{xx} \frac{(1+\mu_2)}{\nu} n^2 \qquad \hat{B}_{13} = \frac{B_{13}}{\bar{D}_{xx}}$$

$$B_{14} = \frac{\nu}{1+\mu_1} n^2$$

$$B_{15} = (2 - \nu + \eta_{t_1} + \eta_{t_2} + \nu \hat{\beta} \zeta_1 \chi_2) n^2 \qquad \hat{B}_{15} = \frac{B_{15}}{\bar{D}_{xx}}$$

$$\hat{B}_{23} = \frac{4cR}{t} \frac{1}{\bar{D}_{xx}} = \frac{B_4}{\bar{D}_{xx}}$$

$$D_2 = \bar{D}_{xx} + \frac{\bar{Q}_{xx}^2}{\bar{H}_{xx}} = B_1$$

$$\bar{D}_{xx} = \frac{4c^2}{Et^3} D_{xx} = 1 + \eta_1 - \frac{(1+\mu_2) \bar{Q}_{xx}^2}{\nu^2 (1-\nu^2) \hat{\beta}}$$

$$\bar{H}_{xx} = Et\, H_{xx} = (1 - \nu^2)\, \hat{\beta}\, (1 + \mu_1)$$

$$\bar{Q}_{xx} = \frac{2c}{t}\, Q_{xx} = \nu\, \hat{\beta}\, \chi_1\, 2\, \frac{c}{t}$$

With $\mu_1 = (1 - \nu^2)\ \frac{A_1}{bt}$ $\qquad$ $\mu_2 = (1 - \nu^2)\ \frac{A_2}{at}$

$$\hat{\beta} = \frac{1}{\alpha_1\ (1+\mu_1)} = \frac{1}{\alpha_2\ (1+\mu_2)}$$

$$\chi_1 = \mu_1\, e_1$$

$$\alpha_1 = \frac{(1+\mu_1)\ (1+\mu_2) - \nu^2}{1 + \mu_1} \qquad \alpha_2 = \frac{(1+\mu_1)\ (1+\mu_2) - \nu^2}{1 + \mu_2}$$

$$\eta_1 = \frac{EI_1}{bD}$$

(See ref. 15, pages 242 - 243)